

# Earth's background free oscillations

KIWAMU NISHIDA

*Earthquake Research Institute, University of Tokyo, 1-1-1 Yayoi, Bunkyo-ku,  
Tokyo 113-0032, Japan.*

**Key Words** seismic hum, ocean infragravity wave, atmospheric turbulence,  
long-period seismology

**Abstract** Earth's background free oscillations known as Earth's hum were discovered in 1998. Excited modes of the oscillations are almost exclusively fundamental spheroidal and toroidal modes from 2 to 20 milli Hz (mHz). Seasonal variations in the source distribution suggest that the dominant sources are ocean infragravity waves in the shallow and deep oceans. A probable excitation mechanism is random shear traction acting on the sea bottom owing to linear topographic coupling of the infragravity waves. Excitation by pressure sources on the earth's surface is also significant for a frequency below 5 mHz. A possible pressure source is atmospheric turbulence, which can cause observed resonant oscillations between the solid modes and atmospheric acoustic modes.

## CONTENTS

INTRODUCTION . . . . .	1
DISCOVERY OF EARTH'S BACKGROUND FREE OSCILLATIONS . . . . .	3
OBSERVATIONS OF SPHEROIDAL MODES . . . . .	4

OBSERVATION OF TOROIDAL MODES . . . . .	6
TEMPORAL AND SPATIAL VARIATIONS IN EXCITATION SOURCES . . . . .	9
ACOUSTIC RESONANCE BETWEEN THE ATMOSPHERE AND SOLID EARTH	12
CUMULATIVE EXCITATION BY SMALL EARTHQUAKES . . . . .	13
EXCITATION BY OCEAN INFRAGRAVITY WAVES . . . . .	13
<i>Nonlinear Coupling between Ocean Infragravity Waves and Seismic Modes</i> . . . . .	15
<i>Topographic Coupling between Ocean Infragravity Waves and Seismic Modes</i> . . . . .	17
EXCITATION BY ATMOSPHERIC TURBULENCE . . . . .	18
SUMMARY POINTS . . . . .	20

## 1 INTRODUCTION

Massive earthquakes generate observable low-frequency seismic waves that propagate many times around the earth. Constructive interference of such waves traveling in opposite directions results in standing waves. The Fourier spectra of observed seismic waves show many peaks in the very low-frequency range ( $<5$  milli Hz (mHz)), which correspond to Earth's normal modes. They contain information about the large-scale internal structure of the earth.

After the 1960 Chilean earthquake, which was the largest earthquake in the 20th century, the Earth's free oscillation was reported for the first time in a memorial paper "Excitation of the free oscillations of the earth by earthquakes" (Benioff et al. 1961). Since then, the eigenfrequencies of these oscillations and their decay rates have been measured and compiled after large earthquakes. With modern seismic instruments, we can now detect major modes of the Earth's free

oscillations after an earthquake with moment magnitude larger than 6.5.

Observations of low-frequency seismic waves were used to constrain the radial and lateral distribution of density, seismic wave speed, and anelastic attenuation within the earth (e.g. Dziewonski & Anderson 1981, Gilbert & Dziewonski 1975, Masters et al. 1996). They also revealed strong evidence that the inner core is solid (Dziewonski 1971). Another important application was the inversion of the centroid moment tensor for large earthquakes (Dziewonski et al. 1981).

Before the first observation of Earth's free oscillations in 1961, many researchers understood that observation of the eigenfrequencies was a key for determining the earth's geophysical properties, following Lord Kelvin's estimation of the molten Earth (Dahlen & Tromp 1998, Thomson 1863). For this detection, Benioff et al. (1959) analyzed not only records of massive earthquakes but also quiet data, which is now recognized as Earth's background free oscillations or Earth's hum, because Benioff et al. (1959) considered the possibility of atmospheric excitation of Earth's free oscillations, but found no such evidence (Kanamori 1998, Tanimoto 2001). The expected signals were so small that their detection was beyond the technological accuracy at that time.

It had long been understood that Earth's free oscillation is a transient phenomenon induced only by large earthquakes, including slow earthquakes, which can selectively excite low-frequency modes and occur several times a year (Beroza & Jordan 1990) and huge volcanic eruptions (Kanamori & Mori 1992, Widmer & Zürn 1992). The possibility of Earth's background free oscillations had been abandoned. Fifty years later, with the development of improved seismic instruments, the Benioff's approach was revived.

Seismic exploration is a powerful tool for the earth's as well as the solar inte-

riors, known as helioseismology (Christensen-Dalsgaard 2002, Gough et al. 1996, Unno et al. 1989). Leighton et al. (1962) showed the first definite observations of solar pulsations in local Doppler velocity with periods of around 5 min. Ulrich (1970) found that the pulsations were generated by standing acoustic waves (equivalent acoustic modes) in the solar interior. These acoustic modes are excited by turbulence at the top of the convective layer (Goldreich & Keeley 1977). Current observations have constrained the solar sound-speed structure to a precision better than 0.5% (Christensen-Dalsgaard 2002)

Similar excitation processes should be expected on solid planets with an atmosphere. Kobayashi (1996) estimated the amplitudes of Earth's background free oscillations using dimensional analysis. Amplitudes of the order of  $\text{ngal}$  ( $10^{-11} \text{ ms}^{-2}$ ) can now be observed by modern seismometers (Peterson 1993). On the basis of the theoretical estimations, the possibility of seismology on Mars has been discussed (Kobayashi & Nishida 1998, Lognonné 2005, Lognonné et al. 2000, 1998b, Nishida et al. 2009, Suda et al. 2002). The theoretical prediction triggered a search for Earth's background free oscillations, as described below.

## 2 DISCOVERY OF EARTH'S BACKGROUND FREE OSCILLATIONS

Following the estimation of Kobayashi (1996), Nawa et al. (1998) reported modal peaks of Earth's background free oscillations, recorded by a superconducting gravimeter at Syowa Station, Antarctica. The discovery triggered a debate because distinct peaks were also caused by the seiches in LützwHolm Bay where the station is located (Nawa et al. 2003, 2000). Immediately after this report Earth's background free oscillations were also confirmed by other sensors:

modified LaCoste–Romberg gravimeter (Suda et al. 1998), STS-1Z seismometer (Kobayashi & Nishida 1998, Tanimoto et al. 1998), and STS-2 seismometer (Widmer-Schmidrig 2003). The studies carefully excluded the effects of large earthquakes (typically  $M_w > 5.5$ ) with the help of earthquake catalogues (Nishida & Kobayashi 1999, Tanimoto & Um 1999). The records of the LaCoste–Romberg gravimeter dated back to 1970s (Agnew & Berger 1978, Suda et al. 1998). For 20 years, Earth's background free oscillations had been accepted as just background noise. Now their existence has been firmly established at more than 200 globally distributed stations. Figure 1 shows a typical example of such data and station locations.

In this study, we cover the background excitation of seismic normal modes from 2 to 20 mHz, referred to as “Earth's background free oscillations”. In sections (Section 3–6), we summarize the observed features of the Earth's background free oscillations. Following that, we will discuss their possible excitation sources: small earthquakes, ocean infragravity waves, and atmospheric turbulence.

### 3 OBSERVATIONS OF SPHEROIDAL MODES

Most of the studies (e.g., Kobayashi & Nishida 1998, Roullet & Wayne 2000, Suda et al. 1998, Tanimoto et al. 1998) used the vertical components of broadband seismometers, because the noise levels in the vertical components are several orders of magnitude lower than those in the horizontal components (Peterson 1993). Stacked spectra on seismically quiet days show distinct modal peaks at eigenfrequencies of the fundamental spheroidal modes. Figure 1 shows a typical example of the spectra of ground acceleration at eight globally distributed stations. The figure shows no significant spatial variation in the observed power spectral den-

sities from 2 to 7 mHz within the accuracy of their instrumental responses of about 10% (Ekström et al. 2006, Hutt 2011). The root mean squared amplitude (RMS) of each mode is of the order of 0.5 ngal with little frequency dependence. The dominance of the fundamental spheroidal modes suggests that the sources were distributed on the earth’s surface. Above 7 mHz we cannot identify distinct modal peaks because the constructive interference of the traveling wave is distorted by lateral heterogeneities of the earth’s internal structure and attenuation. This limitation originates from single-station analysis.

To detect modes above 7 mHz, spatial information of the wave fields should be utilized. Nishida et al. (2002) performed cross-correlation analysis with an assumption of homogeneous and isotropic sources as a stationary stochastic process. This method is a natural extension of the spatial auto-correlation method (Aki 1957) from a semi-infinite case to a spherical one. The resultant wavenumber–frequency spectrum shows a clear branch of fundamental spheroidal modes (Figure 2). Their amplitudes below 7 mHz are consistent with those shown in the single-station analysis. Earth’s background free oscillations can explain existing background noise models (Peterson 1993) from 2 to 20 mHz (Nishida et al. 2002), as shown in Figure 3.

The spatial–time domain representation of the wavenumber–frequency spectrum, displaying the cross-correlation functions between two stations as a function of their separation distance, indicates clear Rayleigh wave propagation from one to another (Snieder 2006). Figure 4 shows the cross-correlation functions bandpass filtered from 3 to 20 mHz. The figure shows the Rayleigh wave as well as the P and S waves. The body wave corresponds to the higher-mode branches of the wavenumber–frequency spectrum (Figure 2). The amplitudes of

the higher modes (body waves) can be explained by surface sources (Fukao et al. 2002). From the cross-correlation functions, the seismic velocity structure of the upper mantle was extracted (Nishida et al. 2009). The method, known as seismic interferometry, has been developed (e.g. Shapiro et al. 2005).

Statistical examination of the excited spheroidal modes indicated three features: (1) standard deviations of the spectra show that the amplitude of each mode fluctuates with time, (2) the total modal signal power of the spectra shows that the oscillations are excited continuously, and (3) the cross-correlation coefficients between the modal powers show that the modes do not correlate, even with adjacent modes (Nishida & Kobayashi 1999). These features show that the sources must be a stationary stochastic process on the entire Earth's surface, which verifies the assumption of the wavenumber–frequency analysis.

The proposed excitation sources of the observed spheroidal modes include commonly assumed random pressure disturbances, either in the atmosphere or the oceans, which cannot generate toroidal modes if the earth is spherically symmetric. Although detection of the toroidal modes is crucial for inferring the excitation mechanism, the high horizontal noise of long-period seismometers had prevented us from detecting them.

#### **4 OBSERVATION OF TOROIDAL MODES**

The most recent data analyses at the quietest sites have revealed the existence of background Love waves from 3 to 20 mHz, which are equivalent to the fundamental toroidal modes. Kurrle & Widmer-Schmidrig (2008) showed the existence of background Love waves from 3.5 to 5.5 mHz using a time domain method based on the auto-correlation functions (Ekström 2001). The observed spheroidal

and toroidal modes exhibited similar horizontal amplitudes. Nishida et al. (2008) showed clear evidence of background Love waves from 0.01 to 0.1 Hz, based on the array analysis of Hi-net tiltmeters in the Japanese islands. The observed kinetic energy of the Love waves was as large as that of the Rayleigh waves throughout the analysis period. Figure 5 shows the results of the array analysis of the observed data at 12.5 mHz. These features suggest that the excitation sources could be represented by random shear traction on the seafloor. Topographic variations in the seafloor, which are perturbations from a spherically symmetric Earth, have a crucial role in these excitations (see section 8 for details).

To qualitatively discuss the force system of the excitation sources, we calculated the synthetic power spectra of acceleration for random shear traction and random pressure on the seafloor using the spherically symmetric Earth model PREM (Dziewonski & Anderson 1981). Here, we consider only the fundamental modes for simplicity. The power spectra of the spheroidal mode  $\hat{\Phi}_v^S$  and  $\hat{\Phi}_h^S$ , and that of the toroidal mode  $\hat{\Phi}_h^T$  are given by

$$\begin{aligned}\hat{\Phi}_v^S(\omega) &= \sum_l \frac{2l+1}{4\pi} |\eta_l^S(\omega)|^2 U_l(R)^2 [\Psi_e^{press}(\omega) U_l(R)^2 + \Psi_e^{shear}(\omega) V_l(R)^2], \\ \hat{\Phi}_h^S(\omega) &= \sum_l \frac{2l+1}{4\pi} |\eta_l^S(\omega)|^2 V_l(R)^2 [\Psi_e^{press}(\omega) U_l(R)^2 + \Psi_e^{shear}(\omega) V_l(R)^2], \\ \hat{\Phi}_h^T(\omega) &= \sum_l \frac{2l+1}{4\pi} |\eta_l^T(\omega)|^2 W_l(R)^4 \Psi_e^{shear}(\omega),\end{aligned}\tag{1}$$

where  $\omega$  is the angular frequency,  $R$  is the radius of the seafloor,  $U_l$  and  $V_l$  are the vertical and horizontal eigenfunctions, respectively, of the  $l$ th fundamental spheroidal mode, and  $W_l$  is the eigenfunction of the fundamental toroidal mode.

The eigenfunctions are normalized as

$$\begin{aligned}\int_0^{R_e} \rho(r) (U_l^2(r) + V_l^2(r)) r^2 dr &= 1 \\ \int_0^{R_e} \rho(r) W_l^2(r) r^2 dr &= 1,\end{aligned}\tag{2}$$

where  $R_e$  is the earth's radius,  $\rho$  is density, and  $r$  is the radius (Dahlen & Tromp 1998). The index  $v$  represents the vertical component and  $h$  represents the horizontal component. Here, the resonance function  $\eta_l^\alpha$  of the  $l$ th mode is defined by

$$\eta_l^\alpha(\omega) = \frac{2\pi R^2 \omega^2}{\left[-\frac{\omega_l^\alpha}{2Q_l^\alpha} - i(\omega_l^\alpha - \omega)\right] \left[-\frac{\omega_l^\alpha}{2Q_l^\alpha} + i(\omega_l^\alpha + \omega)\right]}, \quad (3)$$

where  $\alpha$  indicates the spheroidal mode ( $S$ ) of the toroidal mode ( $T$ ),  $\omega_l^\alpha$  is eigenfrequency of the  $l$ th mode and  $Q_l^\alpha$  is the quality factor of the  $l$ th mode. Here the effective shear traction  $\Psi_e^{shear}$  and the effective random pressure  $\Psi_e^{press}$  (Nishida & Fukao 2007) are defined by

$$\begin{aligned} \Psi_e^{press}(f) &\equiv \frac{L^{press}(\omega)^2}{4\pi R^2} p(\omega) \text{ [Pa}^2\text{/Hz]} \\ \Psi_e^{shear}(f) &\equiv \frac{L^{shear}(\omega)^2}{4\pi R^2} \tau(\omega) \text{ [Pa}^2\text{/Hz]}, \end{aligned} \quad (4)$$

where  $p(\omega)$  is the power spectrum of the random surface pressure,  $\tau(\omega)$  is that of the random surface shear traction,  $L^{press}(\omega)$  is the correlation length of the random surface pressure, and  $L^{shear}(\omega)$  is that of the random surface shear traction.  $\Psi_e^{shear}$  and  $\Psi_e^{press}$  represent the power spectrum of random pressure and the random shear traction on the seafloor per wavenumber, respectively. In equation (1), we also evaluate the excitation by the effective pressure for discussion in following sections.

Here we consider only the random shear traction based on an empirical model (Nishida & Fukao 2007) as

$$\Psi_e^{shear}(f) \sim 7 \times 10^{-6} \left(\frac{f}{f_0}\right)^{-2.3} \text{ [Pa}^2\text{/Hz]}, \quad (5)$$

where  $f_0 = 1$  mHz. The model is slightly modified from that of the effective pressure (Fukao et al. 2002). This model explains the observed vertical components of the fundamental spheroid modes below 6 mHz.

For comparison with the observations, we calculated the spectral ratio between the fundamental toroidal and spheroid modes for the empirical model in Figure 6. The model of the random shear traction can explain the observed amplitude ratios at frequencies around 12 mHz (Nishida et al. 2008). However, at frequencies around 4 mHz, the observed ratios are significantly smaller than that estimated (Kurrle & Widmer-Schmidrig 2008). The model overpredicts the amplitudes of the toroidal mode at 4 mHz. This result suggests that below 5 mHz, we must consider contribution of random surface pressure.

## 5 TEMPORAL AND SPATIAL VARIATIONS IN EXCITATION SOURCES

If the excitation sources of Earth's background free oscillations were oceanic and/or atmospheric in origin, temporal variations in the excitation amplitudes should be observed. Figure 7 shows a spectrogram of mean spectra observed on seismically quiet days from 1991 to 2011. To improve the signal-to-noise ratio, the spectra were stacked over 44 stations for 3 months (90 days); the resultant spectrum was regarded as the average spectrum for the middle of the month. The figure shows persistent excitation of the fundamental spheroidal modes with seasonal variations.

To enhance the signal-to-noise ratio, we stacked all the modes from  ${}_0S_{22}$  to  ${}_0S_{43}$  except for  ${}_0S_{29}$ . Figure 8 shows the annual and semiannual variations (RMS amplitudes) of about 10% with the largest peak in July and a secondary peak in January (Ekström 2001, Nishida et al. 2000, Roult & Wayne 2000, Tanimoto 2001, Tanimoto & Um 1999). We can also identify anomalous variations in one specific mode ( ${}_0S_{29}$ ), which is known as the acoustic coupling modes as discussed in

the next section. The estimated amplitudes were scattered partly because of the heterogeneous source distribution. For further discussion, the spatial distribution of the sources should be inferred. However, the number of available stations was not enough to infer this at the initial stage of the studies.

During the 2000s, increased number of broadband seismometers in the global and regional networks facilitated inferring the distribution on the excitation sources. Rhie & Romanowicz (2004) determined the locations of the excitation sources using two arrays of broadband seismometers, one in California and the other in Japan. Array analyses (Rost & Thomas 2002) is an efficient method for processing large amount of data, partly because the phase differences between the records are a more robustly observed parameters than the amplitudes themselves (Ekström et al. 2006, Hutt 2011). Figure 9 shows the seasonal variations in source locations in the year 2000 by Rhie & Romanowicz (2004). In the northern-hemispheric winter, the strongest sources were located in the northern Pacific Ocean (Figure 9 (a)), whereas in the summer, they were located near the Antarctic Ocean (Figure 9 (b)). Based on a comparison of the seasonal variations with the global distribution of significant wave height in winter (Figure 9 (c)) and summer (Figure 9 (d)), the authors concluded that Earth's background free oscillations were excited by ocean infragravity waves throughout interaction with the seafloor topography. Other studies (Bromirski & Gerstoft 2009, Kurrle & Widmer-Schmidrig 2006, Rhie & Romanowicz 2006, Traer et al 2012) using arrays of vertical components also supported the result that the major sources of the background Rayleigh waves were located in regions around the ocean–continent borders, where the ocean wave height was the highest. An array analysis using horizontal components in Japan (Nishida et al. 2008) showed that the azimuthal

distributions of background Love waves are similar to those of Rayleigh waves. The background surface waves along the continental coast were strongest; the weaker waves with clearly observed amplitudes traveled from the Pacific Ocean and the weakest waves traveled from the Asian continent (Figure 5 (c)). Although these were in good agreement with their spatial distribution, the precise spatial extent of the sources had potential ambiguity because of the use of local or regional datasets (e.g., USArray, F-net, Hi-net).

Cross-correlation analysis is another method used for estimation of source distribution. A cross-correlation function between two stations is highly sensitive to excitation sources randomly distributed in close proximity of the major arc of the great circle path where waves radiating from it interfere constructively while waves radiated from sources off the great circle path interfere destructively (Nishida & Fukao 2007, Snieder 2006). Therefore, if there is any heterogeneity in the spatial distribution of the excitation sources, the observed cross-correlation functions would deviate from the reference. This method was applied for microseisms from 0.025 to 0.2 Hz (Stehly et al. 2006). Here, we note that a frequency–slowness spectrum by the array analysis (e.g. Figure 5 (b)) can be mathematically reconstructed from the cross-correlation functions. These two methods are equivalent in some cases.

To infer the spatial extent of the sources, Nishida & Fukao (2007) modeled the cross-spectra of the vertical components between pairs of stations assuming stationary stochastic excitation of the Rayleigh waves by random surface pressure sources. They fitted the synthetic spectra to yearly averages of observed cross-spectra between pairs of 54 global stations for two-month periods. Figure 10 shows the resulting source distributions from 2 to 10 mHz every two months.

The locations of the strongest sources are consistent with those estimated by the array analysis. This study also showed that the excitation sources are not only localized in shallow oceanic regions but are also distributed over the entire sea surface.

The source distribution of the background Love waves (or toroidal modes) has not yet been inferred because of the high noise levels of the horizontal components. Recent dense networks of broadband seismometers may reveal the distribution in future studies.

## 6 ACOUSTIC RESONANCE BETWEEN THE ATMOSPHERE AND SOLID EARTH

Acoustic coupling between the earth and atmosphere is important when considering the atmospheric excitation of free oscillations of the solid earth (Lognonné et al. 1998a, Watada 1995, Watada & Kanamori 2010). Resonant oscillations are observed at two frequencies: one is the fundamental Rayleigh wave at periods around 270 s ( ${}_0S_{29}$ ) and the other one is the Rayleigh wave at periods around 230 s ( ${}_0S_{37}$ ).  ${}_0S_{29}$  is coupled with a mode along the fundamental branch of the atmospheric acoustic modes, whereas  ${}_0S_{37}$  is coupled with an acoustic mode along the first overtone branch, as shown in Figure 11. This acoustic coupling was observed for the first time when a major eruption of Mt. Pinatubo, the Philippines, occurred on June 15, 1991, (Kanamori & Mori 1992, Widmer & Zürn 1992, Zürn & Widmer 1996). They were recognized as harmonic long-period ground motions at the resonance frequencies associated with the eruption recorded at many stations on the world-wide seismographic networks.

Evidence of acoustic coupling of Earth's background free oscillations can be

found in the presence of two local increased modal amplitudes of these oscillations at angular orders of 29 and 37 (Nishida et al. 2000). Figures 1 and 7 show the two local maxima of the excitation amplitudes. The increase in amplitudes of the two resonant frequencies are found to be around 10~20% of the amplitude of the decoupled modes. These amplitudes are consistent with those estimated from the wavenumber–frequency spectra (Nishida et al. 2002). We note that the coupling mode from the Pinatubo eruption was  ${}_0S_{28}$ , whose angular order is slightly different. The difference may be owing to the local atmospheric structure (Watada & Kanamori 2010). These effects (e.g. wind and temperature) will be addressed in future studies.

The coupled mode  ${}_0S_{29}$  shows a greater annual variation (about 40%) than the oscillations that are decoupled from the atmospheric oscillations (Figure 8). This amplification should depend critically on the extent of the resonance occurring between the solid earth and atmosphere. The eigenfrequencies of the acoustic modes are sensitive to the acoustic structure of the atmosphere, which varies annually. The difference in the amplitude of the annual variation between  ${}_0S_{29}$  and other modes suggests that the annual variation in the acoustic structure is more attuned to the resonant frequencies of the acoustic modes than to those of the seismic modes in the northern-hemispheric summer (“tuning mechanism”; Nishida et al. 2000). The attenuation and eigenfrequency of the acoustic resonance are so sensitive to the local atmospheric structure (Kobayashi 2007) that more quantitative treatment of the coupling is needed for further discussion.

## **7 CUMULATIVE EXCITATION BY SMALL EARTHQUAKES**

In the following sections, we will discuss the possible excitation mechanisms. Most of studies of Earth's background free oscillations excluded seismic records that were disturbed by large earthquakes (e.g., Nishida & Kobayashi 1999, Tanimoto & Um 1999). However, many small earthquakes may induce continuous tiny free oscillations. This possibility was rejected on the basis of a numerical experiment and order of magnitude estimate (Kobayashi & Nishida 1998, Suda et al. 1998, Tanimoto & Um 1999). Using the Gutenberg–Richter law, the modal amplitudes of Earth's free oscillations were estimated to be two or three orders of magnitude smaller than the observed ones. The observed temporal and spatial characteristics also rejected this mechanism.

## **8 EXCITATION BY OCEAN INFRAGRAVITY WAVES**

Shortly after the discovery of Earth's background free oscillations, pressure changes at the ocean bottom due to oceanic swells were suggested as the probable excitation source (Tanimoto 2005, Watada & Masters 2001). Ocean swells in this frequency band are gravity waves often called infragravity waves in deep sea or surf beat in coastal areas. The typical frequency of Earth's background free oscillations of about 0.01 Hz (Figure 3) coincides with a broad peak in the ocean bottom pressure spectrum (e.g. Sugioka et al. 2010, Webb 1998). Rhie & Romanowicz (2004) found that the excitation sources are dominant in the northern Pacific Ocean in the northern-hemispheric winter and in the Circum-Antarctic in the southern-hemispheric winter. The source distribution is consistent with oceanic wave height data. By comparing this result to the oceanic significant wave height data, they concluded that the most probable excitation source is

ocean infragravity waves. Note that the significant wave height does not directly reflect the ocean infragravity waves but the wind waves of a typical frequency of the order of 0.1 Hz.

To discuss the excitation by ocean infragravity waves, we consider the horizontal propagation of ocean infragravity waves. We consider the  $z$ -axis to be positive upward with the undisturbed sea surface at  $z = 0$  and the undisturbed seafloor at  $z = -h$ , as shown in Figure 12 (a). We assume that a sinusoidal wave propagates in the positive  $x$  direction with wavenumber  $k$  and angular frequency  $\omega$ . The phase velocity  $c_0$  is given by

$$c_0 = \sqrt{\frac{g}{k} \tanh kh}, \quad (6)$$

where  $g$  is gravitational acceleration. In the long-wave approximation ( $kh \ll 1$ ), infragravity waves propagate in the horizontal direction with an approximate phase velocity of  $\sqrt{gh}$ . Slower velocities at shallower water depths tend to trap most of the infragravity waves in shallow areas where there are two types of freely propagating infragravity waves: edge and leaky waves. Edge waves are repeatedly refracted to be trapped in close proximity to the shore, whereas leaky waves can propagate to and from deep water (Figure 12 (b)). In the shallow waters of the surf zone, the infragravity waves steepen their fronts with increasing amplitudes, a phenomenon known as surf beat.

Ocean infragravity waves are generated primarily by nonlinear forcing by higher-frequency wind waves with dominant periods around 10 s (Longuet-Higgins & Stewart 1962, Munk 1949). Bowen & Guza (1978) suggested that edge waves might become larger than leaky waves because they are trapped in shallow water (low-velocity region) where strong nonlinear forcing occurs. Mesoscale forcing by the primary wind waves in the deep ocean also generates the ocean infragravity

waves (Uchiyama & McWilliams 2008). Although these studies and observations have improved our knowledge of ocean infragravity waves, these waves are still not been fully understood.

## **8.1 Nonlinear Coupling between Ocean Infragravity Waves and Seismic Modes**

Higher-frequency ocean swells from 0.05 to 0.2 Hz also excite seismic waves. The excited background Love and Rayleigh waves are known as microseisms. The excitation mechanisms of these waves has been firmly established. Microseisms are identified at the primary and double frequencies (Figure 3). Primary microseisms are observed at around 0.08 Hz and have been interpreted as being caused by direct loading of ocean swell onto a sloping beach (Haubrich et al. 1963). The typical frequency of the secondary microseisms is about 0.15 Hz approximately double the typical frequency of ocean swells, indicating the generation of the former through nonlinear wave–wave interaction of the latter (Kedar et al. 2008, Longuet–Higgins 1950). There are several reports of background Love waves in the microseismic bands, where the energy ratio of Love to Rayleigh waves is much higher for the primary microseisms than for the secondary microseisms (Friedrich et al. 1998, Nishida et al. 2008). Because the ratio of Love to Rayleigh waves for primary microseisms is similar to that of Earth's background free oscillations at 10 mHz, the low-frequency components of primary microseisms (Kurrle & Widmer-Schmidrig 2010) may be related to the excitation of Earth's background free oscillations.

Webb (2007) extended the Longuet–Higgins mechanism of secondary microseisms to the excitation of Earth's background free oscillations with a correction

of the ellipticity of the particle motion of the infragravity waves (Tanimoto 2007, 2010, Webb 2008). He concluded that the infragravity waves trapped in shore regions are dominant sources of Earth's background free oscillations, although the excitation by the infragravity waves in regions of oceanic basins cannot be neglected (Webb 2008).

For a better understanding of this mechanism, we consider a simplified case shown Figure 12 (b). When two regular wave trains traveling in opposite directions with displacement amplitude of the sea surface  $\zeta$  and frequency  $\omega$  interact, the second-order pressure pressure fluctuation  $\delta p$  can be approximated by  $-2\rho\phi_\zeta(f)\omega^2\Delta f$ , where  $\phi_\zeta(f)$  is the power spectra of the displacement amplitude of the sea surface. The power spectra of the pressure fluctuations  $p$  and their correlation length  $L^{press}$  can then be roughly estimated as

$$p(f) \sim \delta p^2/\Delta f [\text{Pa}^2/\text{Hz}], \quad (7)$$

$$L^{press}(f) \sim \lambda = 10^5 [\text{m}]. \quad (8)$$

In particular, the estimation of the correlation length has potential ambiguity. Inserting of these parameters into equation (1) and (4) we can estimate the amplitudes of Earth's background free oscillations that were consistent with the observed amplitudes of the background Rayleigh waves from 5 to 20 mHz (Tanimoto 2007, 2010, Webb 2008).

The drawback of this mechanism is that it cannot explain the observed background Love waves because the pressure sources cannot excite Love waves in a spherically symmetric structure (Tanimoto 2010). In addition, the mechanisms cannot explain the observed typical frequency of Earth's background free oscillations of about 0.01 Hz, because the typical frequency should be double the frequency of about 0.02 Hz owing to the nonlinear effect.

We cannot rule out this possibility for frequencies below 5 mHz, because pressure sources are also significant in this frequency range (Figure 3). Although most of studies focussed on nonlinear forcing of seismic modes by ocean infragravity waves, the nonlinear forcing by the primary higher-frequency wind waves at around 0.1 Hz may not be negligible. The mechanism should be addressed in further studies.

## 8.2 Topographic Coupling between Ocean Infragravity Waves and Seismic Modes

A possible excitation mechanism of background Love and Rayleigh waves in the frequency range of 2–20 mHz is linear topographic coupling between ocean infragravity waves and seismic surface waves (Fukao et al. 2010, Nishida et al. 2008, Saito 2010). The wavelengths of infragravity waves in this frequency range are of the order of 10–40 km in the deep ocean. The seafloor topography with wavelengths of this order is dominated by abyssal hills on the ocean floor. The coupling occurs efficiently when wavelength of the infragravity waves at the frequency  $\lambda$  and the horizontal scale of the topography match each other. The topographic coupling generates a random distribution of point-like tangential forces on the sea floor. Fukao et al. (2010) assumed that a random distribution of triangular hills. In this case, the power spectrum of the random shear traction  $\tau$  and the correlation length  $L^{shear}$  can be estimated as

$$\tau(f) \sim p^{ocean}(f)C \frac{H^2}{\lambda^2} [\text{Pa}^2/\text{Hz}], \quad (9)$$

$$L^{shear}(f) \sim \lambda [\text{m}], \quad (10)$$

where  $C$  is a non-dimensional statistical parameter of hill's distribution,  $H$  is the height of the hill whose horizontal scale is  $\lambda$ , and  $p^{ocean}$  is the power spectrum

of the pressure fluctuations on the seafloor (Figure 12 (a)). We should note that this mechanism generates only horizontal force but no vertical force (Fukao et al. 2010). Inserting these parameters into equation (1) and (4), we obtained the estimated amplitudes that were consistent with the observed amplitudes of the background Love and Rayleigh waves from 5 to 20 mHz. They can explain the observed amplitude ratio between the Love and Rayleigh waves (Fukao et al. 2010) as shown in Figure 6, although there are still ambiguities regarding the assumed parameters. The mechanism can also explain observed spatial extent of the sources.

## 9 EXCITATION BY ATMOSPHERIC TURBULENCE

An atmospheric excitation mechanism was first proposed by Kobayashi (1996) on the analogy of helioseismology. Atmospheric turbulence and/or cumulus cloud convection (Shimazaki & Nakajima 2009) in the troposphere cause atmospheric pressure disturbances. They act on the earth's surface and persistently induce spheroidal modes of the earth as shown in Figure 12 (c). According to his theory, the excitation sources can be characterized by stochastic parameters of atmospheric turbulence: one is the power spectra of the pressure disturbances  $p(f)$  and the other is their correlation length  $L^{press}(f)$ . These pressure sources can excite only Rayleigh waves. Therefore, this mechanism is applicable below 5 mHz. A quantitative comparison was made between the atmospheric pressure disturbance and Earth's background free oscillations (Fukao et al. 2002, Kobayashi & Nishida 1998, Tanimoto & Um 1999) and an empirical model was defined by

$$p(f) = 4 \times 10^3 \times \left(\frac{f}{f_0}\right)^{-2} [\text{Pa}^2/\text{Hz}] \quad (11)$$

$$L^{press}(f) = 600 \times \left(\frac{f}{f_0}\right)^{-0.12} \text{ [m]}. \quad (12)$$

There are still ambiguities in this estimation because the global observation of the atmospheric turbulence lacks in this frequency range. In particular, their spatial structure strongly depends on the buoyancy frequency in the lowermost atmospheric structure that is too complex to evaluate.

The atmospheric excitation mechanism can also explain observed resonant oscillations between the solid modes and acoustic modes at the two frequencies, 3.7 and 4.4 mHz (Kobayashi et al. 2008). Webb (2008) pointed out that ocean infragravity waves could excite low-frequency atmospheric acoustic waves through nonlinear interaction, as in microbaroms, at frequencies of about 0.2 Hz (Arendt & Fritts 2000). However, observed low-frequency infrasounds below 10 mHz were related to atmospheric phenomena: convective storms, and atmospheric turbulence in mountain regions (Georges 1973, Gossard & Hooke 1975, Jones & Georges 1976, Nishida et al. 2005). The acoustic resonance observed at the two frequencies suggests that atmospheric disturbances contribute to the excitation of Earth's background free oscillation.

Atmospheric internal gravity waves are another possible source of excitation. The same principles of topographic coupling and nonlinear forcing of ocean infragravity waves may be applied to atmospheric internal gravity waves. Below 10 mHz, the influence of internal gravity waves becomes dominant in the lower atmosphere (Nishida et al. 2005), although this depends strongly on local stratification. Because their amplitudes are of the order of  $10^4$  [Pa<sup>2</sup>/Hz], these excitation mechanisms may not be negligible. These mechanisms should be addressed in a future study.

## 10 SUMMARY POINTS

1. Earth's background free oscillations from 2 to 20 mHz are observed at globally distributed stations.
2. Excited modes of the oscillations are almost exclusively fundamental spheroidal and toroidal modes. Amplitudes of the toroidal modes are larger than those of the spheroidal modes.
3. During the 2000s, increased number of broadband seismometers in the global and regional networks facilitated inferring temporal variations in the source distribution. They suggest that ocean infragravity waves are dominant sources of the oscillations.
4. A possible excitation mechanism of the oscillations is random shear traction on the Earth's surface, which owes to linear topographic coupling between ocean infragravity waves and seismic modes.
5. Pressure sources is also significant for the oscillations below 5 mHz. Acoustic resonance between the atmosphere and solid earth at 3.7 and 4.4 mHz suggests that atmospheric disturbances contribute to the excitation. Another possibility is nonlinear forcing of the seismic modes by ocean infragravity waves.

## DISCLOSURE STATEMENT

The authors are not aware of any affiliations, memberships, funding, or financial holdings that might be perceived as affecting the objectivity of this review.

**ACKNOWLEDGMENTS**

Yoshio Fukao, Naoki Kobayashi, and Kazunari Nawa provided valuable comments that improved the paper. This research was partially supported by JSPS KAKENHI (22740289). We are grateful to a number of people who have been associated with IRIS since its inception for maintaining the networks and making the data readily available.

**LITERATURE CITED**

- Agnew DC, Berger J. 1978. Vertical Seismic Noise at Very Low Frequencies. *J. Geophys. Res.* 83:5420–5424
- Aki K. 1957. Space and time Spectra of stationary stochastic waves, with special reference to microseisms. *Bull. Earthq. Res. Inst.* 35:415–457
- Arendt S, Fritts DC. 2000. Acoustic radiation by ocean surface waves. *J. Fluid Mech.* 415:1–21
- Benioff H, Harrison J, LaCoste L, Munk WH, Slichter LB. 1959. Searching for the Earth's free oscillations. *J. Geophys. Res.* 64:1334
- Benioff H, Press F, Smith S. 1961. Excitation of the Free Oscillations of the Earth by Earthquakes. *J. Geophys. Res.* 66:605–619
- Beroza G, Jordan T. 1990. Searching for slow and silent earthquakes using free oscillations. *J. Geophys. Res.* 95:2485–2510
- Bowen A, Guza R. 1978. Edge waves and surf beat. *J. Geophys. Res.* 83:913–1920
- Bromirski PD, Gerstoft P. 2009. Dominant source regions of the Earth's hum are coastal. *Geophys. Res. Lett.* 36:1–5
- Christensen-Dalsgaard Jr. 2002. Helioseismology. *Rev. Mod. Phys.* 74:1073–1129

- Dahlen FA, Tromp J. 1998. *Theoretical Global Seismology*. Princeton: Princeton University Press. 1025 pp.
- Dziewonski A. 1971. Overtones of Free Oscillations and the Structure of the Earth's Interior. *Science* 172:1336–1338
- Dziewonski A, Anderson D. 1981. Preliminary reference Earth model. *Phys. Earth Planet. Inter.* 25:297–356
- Dziewonski A, Chou T, Woodhouse J. 1981. Determination of Earthquake Source Parameters From Waveform Data for Studies of Global and Regional Seismicity. *J. Geophys. Res.* 86:2825–2852
- Ekström G. 2001. Time domain analysis of Earth's long-period background seismic radiation. *J. Geophys. Res.* 106:26483–26494
- Ekström G, Dalton CA, Nettles M. 2006. Long-period Instrument Gain at Global Seismic Stations. *Seismol. Res. Lett.* 77:12–22
- Friedrich A, Krüger F, Klinge K. 1998. Ocean-generated microseismic noise located with the gräfenberg array. *J. Seismol.* 2:47–64
- Fukao Y, Nishida K, Kobayashi N. 2010. Seafloor topography, ocean infragravity waves, and background Love and Rayleigh waves. *J. Geophys. Res.* 115:B04302
- Fukao Y, Nishida K, Suda N, Nawa K, Kobayashi N. 2002. A theory of the Earth's background free oscillations. *J. Geophys. Res.* 107:2206
- Georges TM. 1973. Infrasound from Convective Storms: Examining the Evidence. *Rev. Geo. Space Phys.* 11:571–594
- Gilbert F, Dziewonski AM. 1975. An application of normal mode theory to the retrieval of structural parameters and source mechanisms from seismic spectra. *Phil. Trans. R. Soc. Lond. A* 278:187–269

- Goldreich P, Keeley AD. 1977. Solar seismology. II. The stochastic excitation of the Solar p-modes by turbulent convection. *Astrophys. J.* 212:243–251
- Gossard EE, Hooke W. 1975. *Waves in The Atmosphere*. Amsterdam: Elsevier. 442 pp.
- Gough D, Leibacher J, Scherrer P, Toomre J. 1996. Perspectives in Helioseismology. *Science* 272:1281–1283
- Haubrich R, Munk W, Snodgrass F. 1963. Comparative spectra of microseisms and swell. *Bull. Seismol. Soc. Am.* 53:27–37
- Hutt C. 2011. Some Possible Causes of and Corrections for STS-1 Response Changes in the Global Seismographic Network. *Seismol. Res. Lett.* 82:560–571
- Jones RM, Georges TM. 1976. Infrasound from convective storms. III. propagation to the ionosphere. *J. Acoust. Soc. Am.* 59:765–779
- Kanamori H. 1998. Shaking without quaking. *Science* 279:2063–2064
- Kanamori H, Mori J. 1992. Harmonic excitation of mantle Rayleigh waves by the 1991 eruption of Mount Pinatubo Philippines. *Geophys. Res. Lett.* 19:721–724
- Kedar S, Longuet-Higgins M, Webb F, Graham N, Clayton R, Jones C. 2008. The origin of deep ocean microseisms in the Northern Atlantic Ocean. *Proc. R. Soc. A* 464:777–793
- Kobayashi N. 1996. Oscillations of solid planets excited by atmospheric random motions. *Fall Meeting of the Japanese Soc. for Planet. Sci.*. Fukuoka (Abstr.)
- Kobayashi N. 2007. A new method to calculate normal modes. *Geophys. J. Int.* 168:315–331
- Kobayashi N, Kusumi T, Suda N. 2008. Infrasounds and background free oscillations. *Proc. 8th International Conference on Theoretical and Computa-*

- tional Acoustics, Heraklion, Crete, Greece, 2-5 July 2007*, pp. 105–114. eds. M Taroudakis, P Papadakis. E-MEDIA University of Crete
- Kobayashi N, Nishida K. 1998. Continuous excitation of planetary free oscillations by atmospheric disturbances. *Nature* 395:357–360
- Kurrle D, Widmer-Schmidrig R. 2006. Spatiotemporal features of the Earth's background oscillations observed in central Europe. *Geophys. Res. Lett.* 33:2–5
- Kurrle D, Widmer-Schmidrig R. 2008. The horizontal hum of the Earth: A global background of spheroidal and toroidal modes. *Geophys. Res. Lett.* 35:L06304
- Kurrle D, Widmer-Schmidrig R. 2010. Excitation of long-period Rayleigh waves by large storms over the North Atlantic Ocean. *Geophys. J. Int.* 183:330–338
- Leighton R, Noyes R, Simon G. 1962. Velocity Fields in the Solar Atmosphere. I. Preliminary Report. *Astrophys. J.* 135:474
- Lognonné P. 2005. Planetary seismology. *Ann. Rev. Earth Planet. Sci.* 33:571–604
- Lognonné P, Clévéde E, Kanamori H. 1998a. Computation of seismograms and atmospheric oscillations by normal-mode summation for a spherical earth model with realistic atmosphere. *Geophys. J. Int.* 135:388–406
- Lognonné P, Giardini D, Banerdt B, Gagnepain-Beyneix J, Mocquet A, et al. 2000. The NetLander very broad band seismometer. *Planet. Space Sci.* 48:1289–1302
- Lognonné P, Zharkov VN, Karczewski JF, Romanowicz B, Menvielle M, et al. 1998b. The seismic OPTIMISM experiment. *Planet. Space Sci.* 46:739–747
- Longuet-Higgins M. 1950. A theory of the origin of microseisms. *Phil. Trans. Roy. Soc. Lond. A* 243:1–35

- Longuet-Higgins M., Stewart R. 1962. Radiation stress and mass transport in gravity waves with application to surf-beats. *J. Fluid Mech.* 13:481–504
- Masters G, Johnson S, Laske G, Bolton H, Davies JH. 1996. A shear-velocity model of the mantle. *Phil. Trans. R. Soc. Lond. A* 354:1385–1411
- Munk W. 1949. Surf beats. *EOS Trans. AGU.* 30:849–854
- Nawa K, Suda N, Aoki S, Shibuya K, Sato T, Fukao Y. 2003. Sea level variation in seismic normal mode band observed with on-ice GPS and on-land SG at Syowa Station, Antarctica. *Geophys. Res. Lett.* 30(7):1402
- Nawa K, Suda N, Fukao Y, Sato T., Tamura, Y., Shibuya, K., McQueen, H., Virtanen, H., Kaariainen, J. 2000. Incessant excitation of the earth's free oscillations: global comparison of superconducting gravimeter records. *Phys. Earth Planet. Inter.* 120:289–297
- Nawa K, Suda N, Fukao Y, Sato T, Aoyama Y, Shibuya K. 1998. Incessant excitation of the Earth's free oscillations. *Earth Planets Space* 50:3–8
- Nishida K, Fukao Y. 2007. Source distribution of Earth's background free oscillations. *J. Geophys. Res.* 112:B06306
- Nishida K, Fukao Y, Watada S, Kobayashi N, Tahira M, et al. 2005. Array observation of background atmospheric waves in the seismic band from 1 mHz to 0.5 Hz. *Geophys. J. Int.* 162:824–840
- Nishida K, Kawakatsu H, Fukao Y, Obara K. 2008. Background Love and Rayleigh waves simultaneously generated at the Pacific Ocean floors. *Geophys. Res. Lett.* 35:L16307
- Nishida K, Kobayashi N. 1999. Statistical features of Earth's continuous free oscillations. *J. Geophys. Res.* 104:28741–28750

- Nishida K, Kobayashi N, Fukao Y. 2000. Resonant Oscillations Between the Solid Earth and the Atmosphere. *Science* 287:2244–2246
- Nishida K, Kobayashi N, Fukao Y. 2002. Origin of Earth’s ground noise from 2 to 20 mHz. *Geophys. Res. Lett.* 29:1413
- Nishida K, Montagner JP, Kawakatsu H. 2009. Global surface wave tomography using seismic hum. *Science* 326:112
- Peterson J. 1993. Observations and modeling of seismic background noise. *U.S. Geol. Surv. Open File Rep.* 93-322:1
- Rhie J, Romanowicz B. 2006. A study of the relation between ocean storms and the Earth’s hum. *Geochem. Geophys. Geosyst.* 7:Q10004
- Rhie J., Romanowicz B. 2004. Excitation of Earth’s continuous free oscillations by atmosphere-ocean-seafloor coupling. *Nature* 431:552–556
- Rost S, Thomas C. 2002. Array seismology: methods and applications. *Rev. Geophys.* 40:1–2
- Roult G, Wayne C. 2000. Analysis of background free oscillations and how to improve resolution by subtracting the atmospheric pressure signal. *Phys. Earth Planet. Inter.* 121:325–338
- Saito T. 2010. Love-wave excitation due to the interaction between a propagating ocean wave and the sea-bottom topography. *Geophys. J. Int.* 182:1515–1523
- Shapiro N, Campillo M, Stehly L, Ritzwoller M. 2005. High-resolution surface-wave tomography from ambient seismic noise. *Science* 307:1615–1618
- Shimazaki, K, Nakajima, K. 2009. Oscillations of Atmosphere–Solid Earth Coupled System Excited by the Global Activity of Cumulus Clouds *Eos Trans. AGU* 90(52), Fall Meet. Suppl., Abstract S23A-1734

- Snieder R. 2006. Retrieving the Green's function of the diffusion equation from the response to a random forcing. *Phys. Rev. E* 74:046620
- Stehly L, Campillo M, Shapiro NM. 2006. A study of the seismic noise from its long-range correlation properties. *J. Geophys. Res.* 111:B10306
- Suda N, Nawa K, Fukao Y. 1998. Earth's background free oscillations. *Science* 279:2089–2091
- Suda, M, Mitani, C, Kobayashi, N, Nishida, K. 2002, Theoretical Calculation of Mars' Background Free Oscillations *Eos Trans. AGU* 83(47), Fall Meet. Suppl., Abstract S12A-1186
- Sugioka H, Fukao Y, Kanazawa T. 2010. Evidence for infragravity wave-tide resonance in deep oceans. *Nature comm.* 1:84
- Tanimoto T. 2001. Continuous free oscillations: atmosphere-solid earth coupling. *Ann. Rev. Earth Planet. Sci.* 29:563–584
- Tanimoto T. 2005. The oceanic excitation hypothesis for the continuous oscillations of the earth. *Geophys. J. Int.* 160:276–288
- Tanimoto T. 2007. Excitation of normal modes by non-linear interaction of ocean waves. *Geophys. J. Int.* 168:571–582
- Tanimoto T. 2010. Equivalent forces for colliding ocean waves. *Geophys. J. Int.* 181:468–478
- Tanimoto T, Um J. 1999. Cause of continuous oscillations of the Earth. *J. Geophys. Res.* 104:28723–28739
- Tanimoto T, Um J, Nishida K, Kobayashi N. 1998. Earth's continuous oscillations observed on seismically quiet days. *Geophys. Res. Lett.* 25:1553–1556

- Thomson W. 1863. On the Rigidity of the Earth. *Phil. Trans. R. Soc. Lond.* 153:573–582
- Traer J, Gerstoft P, Bromirski PD, Shearer PM. 2012. Microseisms and hum from ocean surface gravity waves. *J. Geophys. Res.*, 117:B11307
- Uchiyama Y, McWilliams JC. 2008. Infragravity waves in the deep ocean: Generation, propagation, and seismic hum excitation. *J. Geophys. Res.* 113:C07029
- Ulrich R. 1970. The five-minute oscillations on the solar surface. *Astrophys. J.* 162:993
- Unno W, Osaki Y, Ando H, Saio H, Shibahashi H. 1989. *Nonradial Oscillations of Stars* Tokyo: Tokyo University Press. 330 pp. 2nd ed.
- Watada S. 1995. *Part I: Near-source Acoustic Coupling Between the Atmosphere and the Solid Earth During Volcanic Eruptions*. Ph.D. thesis, California Institute of Technology
- Watada S, Kanamori H. 2010. Acoustic resonant oscillations between the atmosphere and the solid earth during the 1991 Mt. Pinatubo eruption. *J. Geophys. Res.* 115:B12319
- Watada S, Masters G. 2001. Oceanic excitation of the continuous oscillations of the Earth. *Eos Trans. AGU* 82(47), Fall Meet. Suppl., Abstract S32A-0620
- Webb SC. 1998. Broadband seismology and noise under the ocean. *Rev. Geophys.* 36:105–142
- Webb SC. 2007. The Earth's 'hum' is driven by ocean waves over the continental shelves. *Nature* 445:754–6
- Webb SC. 2008. The Earth's hum: the excitation of Earth normal modes by ocean waves. *Geophys. J. Int.* 174:542–566

Widmer R, Zürn W. 1992. Bichromatic excitation of long-period Rayleigh and air waves by the Mount Pinatubo and El Chichon volcanic eruptions. *Geophys. Res. Lett.* 19:765–768

Widmer-Schmidrig R. 2003. What Can Superconducting Gravimeters Contribute to Normal-Mode Seismology? *Bull. Seismol. Soc. Am.* 93:1370–1380

Zürn W, Widmer R. 1995. On noise reduction in vertical seismic records below 2 mHz using local barometric pressure. *Geophys. Res. Lett.* 22:3537–3540

Zürn W, Widmer R. 1996. Worldwide observation of bichromatic long-period Rayleigh waves excited during the June 15, 1991, eruption of Mount Pinatubo. In *Fire and Mud, Eruptions of Mount Pinatubo, Philippines*, eds. C Newhall, JR Punongbayan, 615–624. Seattle: Univ. Washington Press. 1126 pp.

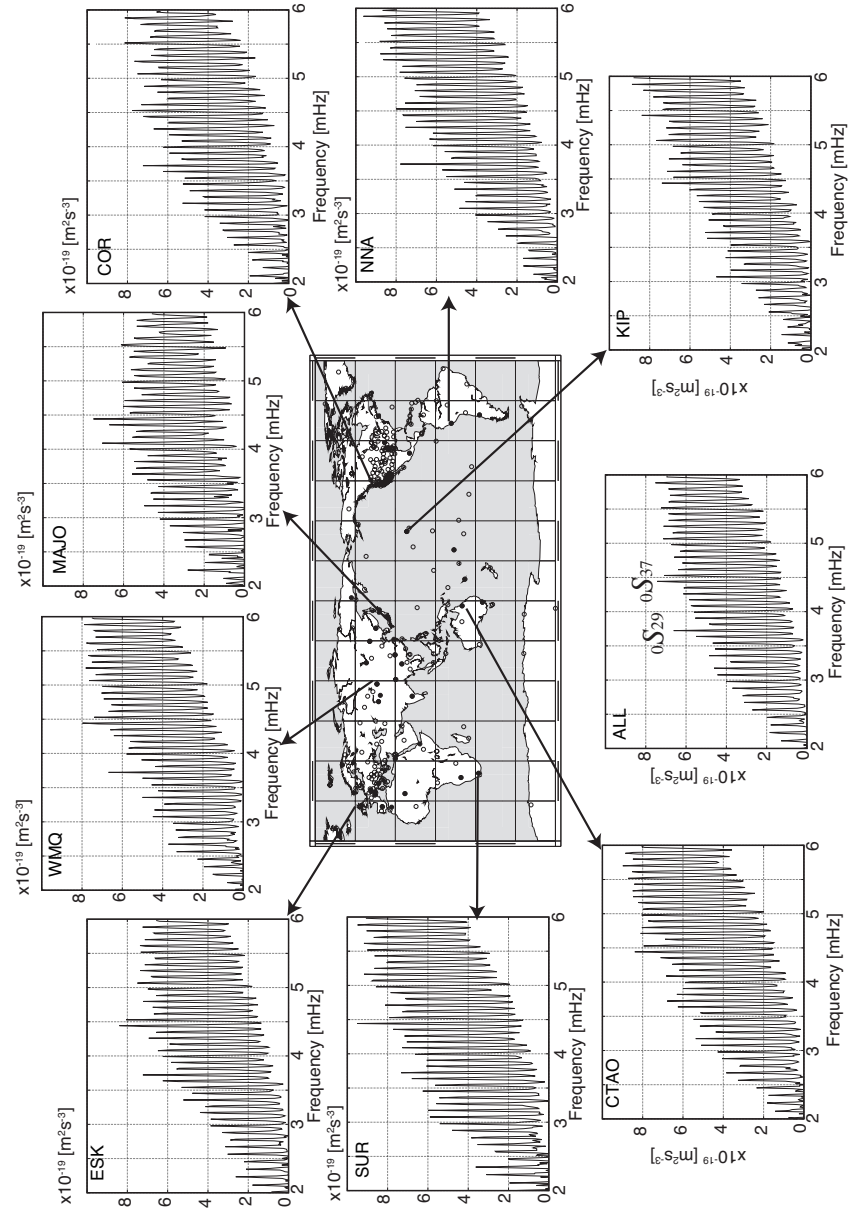


Figure 1: Typical example of power spectra of ground acceleration on seismically quiet days from 1990 to 2011 at 8 stations. Each modal peak corresponds to an eigenfrequency of a fundamental spheroidal mode. The station locations are also shown in the map. We subtracted the local noise due to Newtonian attraction of atmospheric pressure (Zürn & Widmer 1995) and instrumental noise (Fukao et al. 2002, Nishida & Kobayashi 1999). Closed circles on the map show the 44 stations of STS seismometers used for the calculation of the spectrogram shown in Figure 7; open circles show the 283 stations of STS seismometers used for the calculation of the wavenumber–frequency spectrum shown in Figure 2.

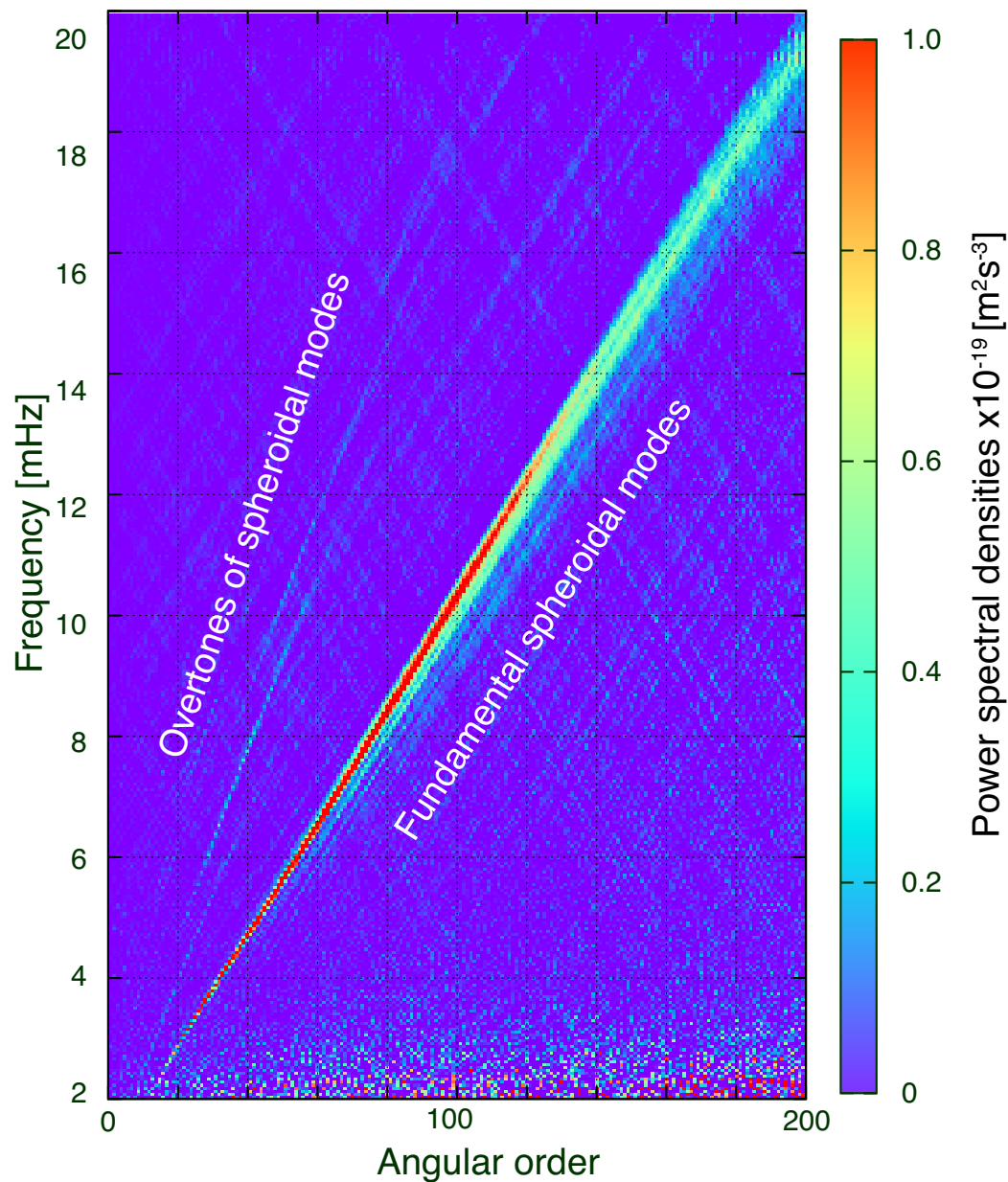


Figure 2: Wavenumber–frequency spectrum (Nishida et al. 2002) calculated from vertical components of 283 STS seismometers. Station locations are shown in Figure 1. Fundamental spheroidal modes as well as overtones are shown. In particular, at higher frequencies, many stripes appear parallel to the fundamental mode branch due to their spectral leakages. They are caused by the incomplete station distribution and lateral heterogeneities of the earth's structure.

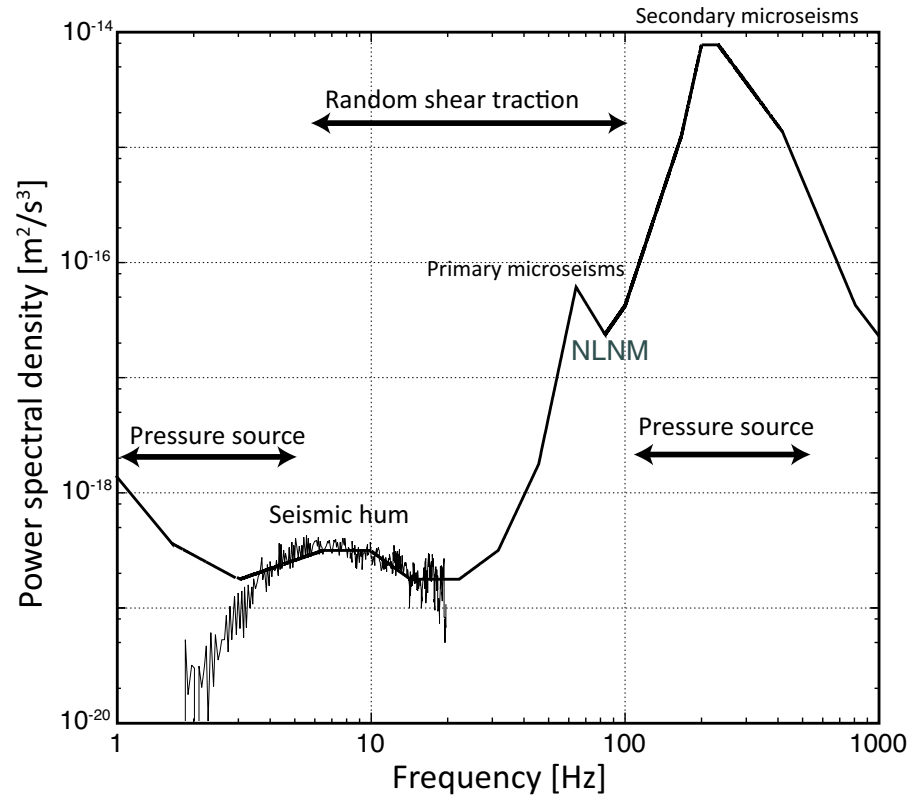


Figure 3: Comparison of the PSDs of the background free oscillations (solid line; Nishida et al. 2002) to those of the background noise (broken line) in the New Low Noise Model (NLNM) (Peterson 1993). They coincide in almost almost the entire seismic passband from 2 to 20 mHz. The force systems of the excitation sources (Fukao et al. 2010, Nishida et al. 2008) are also shown.

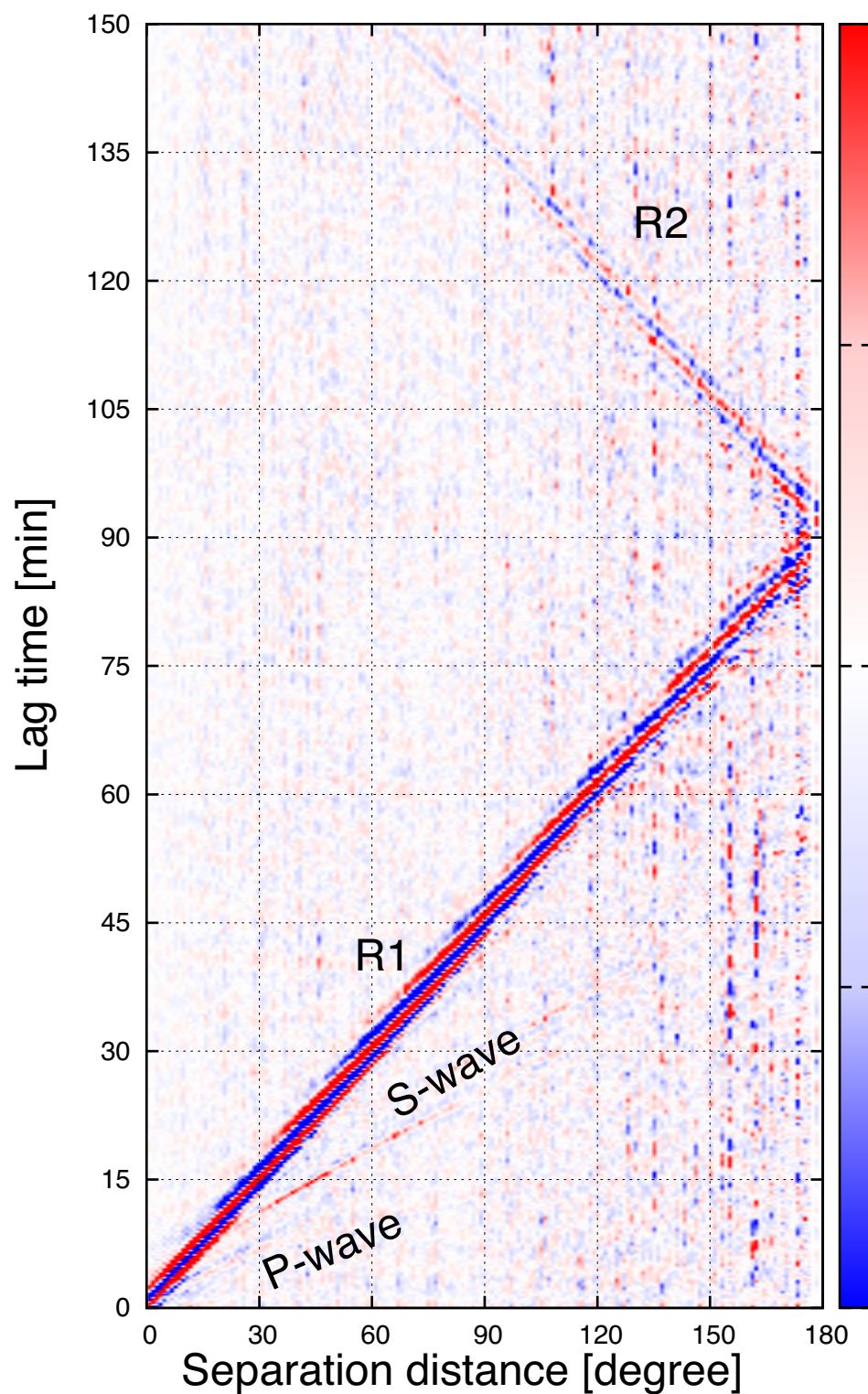


Figure 4: Stacked cross-correlation functions every  $0.5^\circ$  bandpass filtered from 2 to 20 mHz. Seismograms were recorded at stations shown in Figure 1 (open and closed circles). R1 and R2 indicate Rayleigh wave propagation along the minor arc and major arc, respectively. Only the time-symmetric part of cross-correlation functions is shown for simplicity.

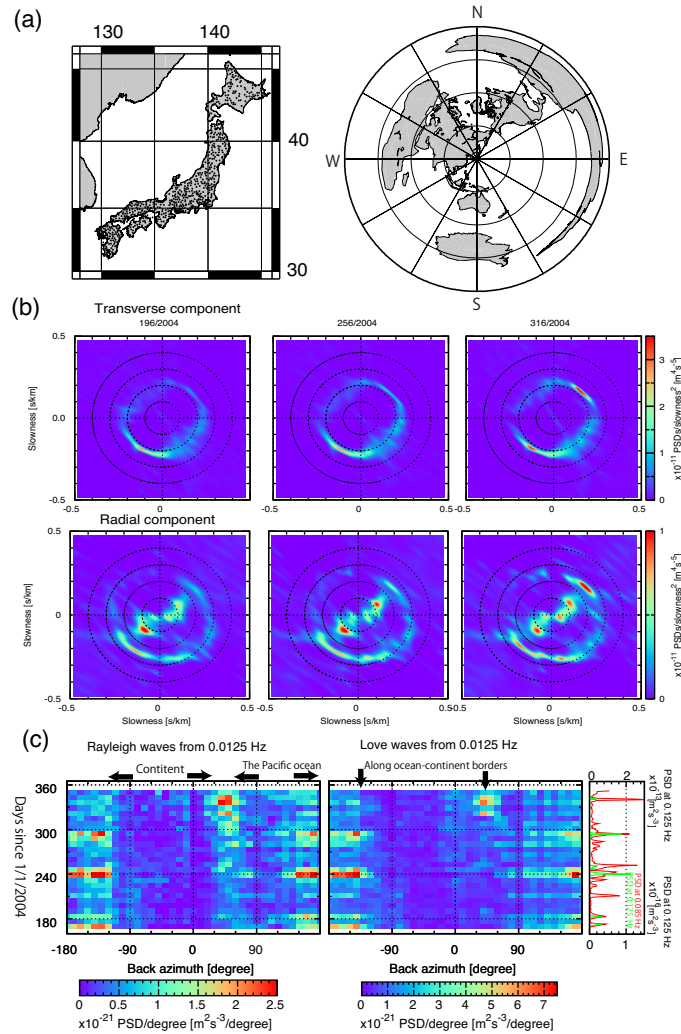


Figure 5: (a) Location map of 679 Hi-net tiltmeters and the distribution of continents and oceans in the azimuthal projection from the center of the Hi-net array. (b) Frequency–slowness spectra at 0.0125 Hz, calculated for every 60 days from 166/2004–346/2004. (c) Azimuthal variations of Love and Rayleigh-wave amplitudes at 0.0125 Hz as functions of time showing the similar azimuthal patterns. The right column indicates the temporal change of amplitudes of primary microseisms (mean power spectral densities from 0.08 to 0.09 Hz), and secondary microseisms (and those from 0.12 to 0.125 Hz) showing the activity pattern similar to those of Love and Rayleigh waves at 0.0125 Hz. Taken from Nishida et al. (2008).

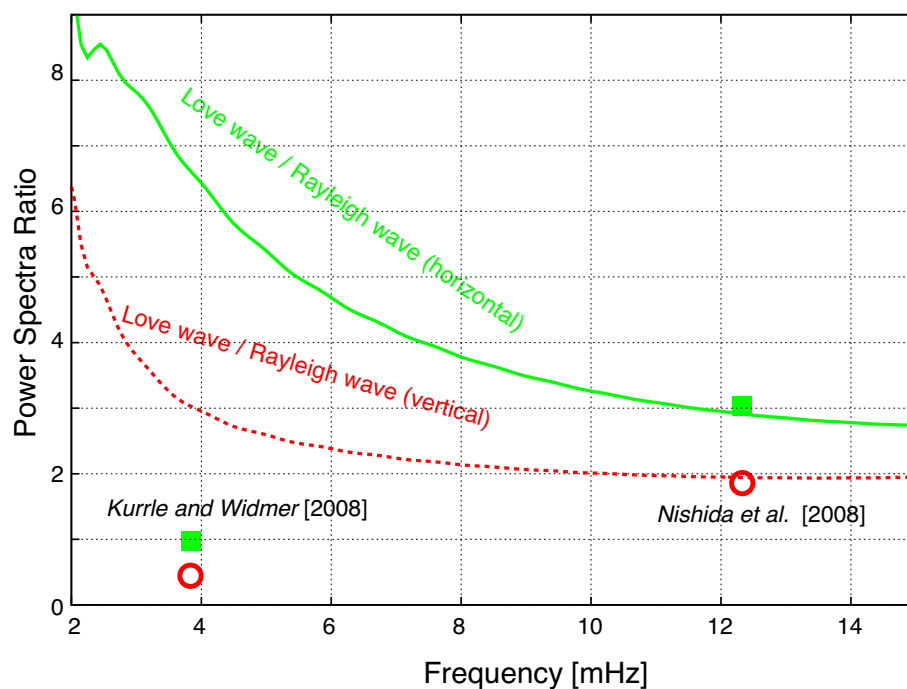


Figure 6: Ratios between background Love and Rayleigh waves. The ratio between the synthetic power spectrum of the fundamental Love wave and that of the horizontal component (solid green line) and vertical component (dashed red line) of the fundamental Rayleigh wave. The results observed by Kurrle & Widmer-Schmidrig (2008) and Nishida et al. (2008) are also shown. Green closed squares and red open circles show the ratio between the Love wave and the horizontal and vertical components of the Rayleigh wave, respectively.

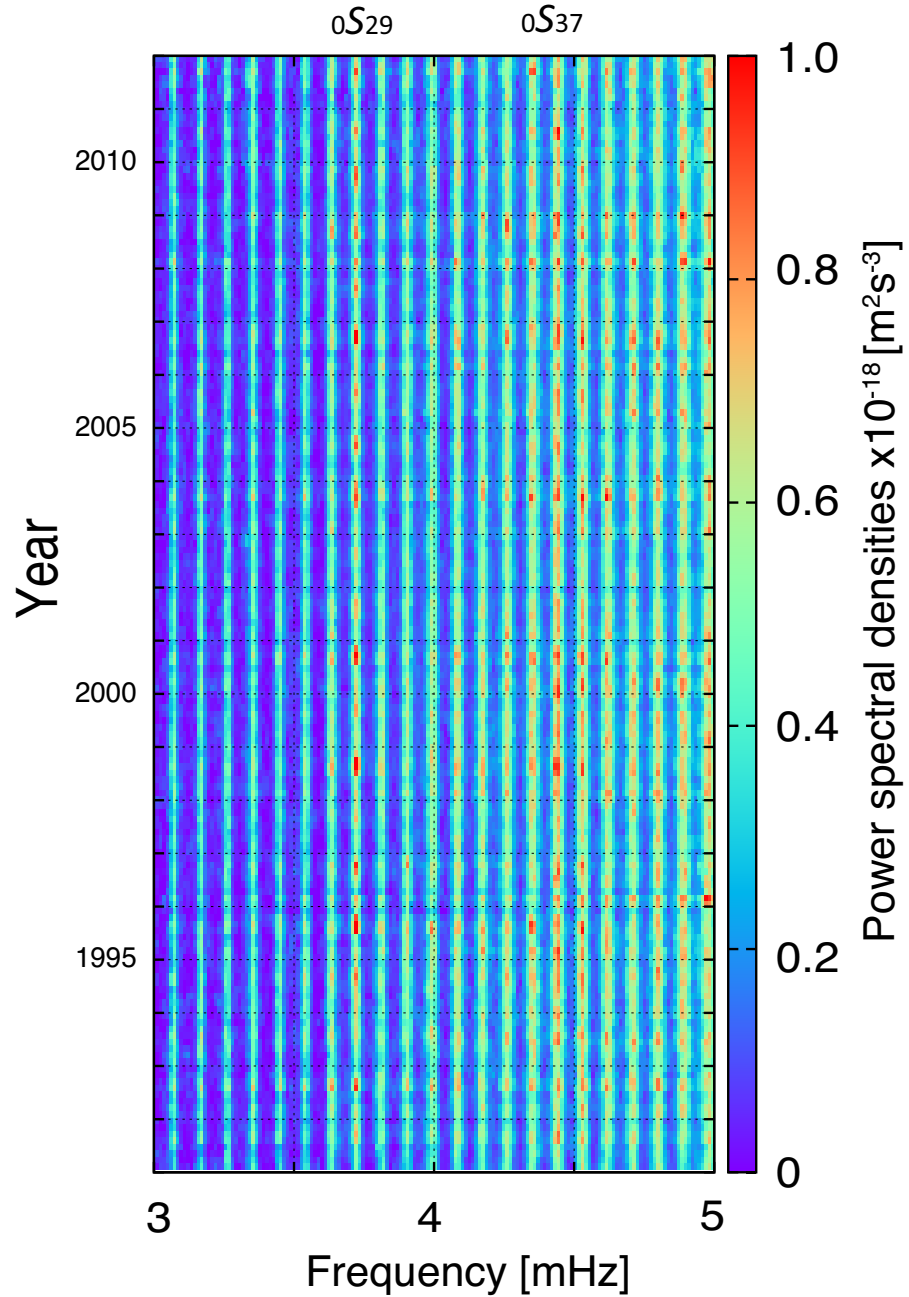


Figure 7: Spectrogram of the seismically quiet days from 1990 to 2011, showing successive monthly spectra each spectrum is an average of the 1-day spectra over 90 days and over 44 stations shown in Figure 1. We subtracted the local noise due to Newtonian attraction of atmospheric pressure (Zürn & Widmer 1995) and instrumental noise (Fukao et al. 2002, Nishida & Kobayashi 1999). The figure shows only relatively narrow frequency range from 3 to 5 mHz. The vertically intense lines with approximately regular intervals correspond to the spectral peaks of fundamental spheroidal modes. An apparent annual variation is observed (Nishida et al. 2000).

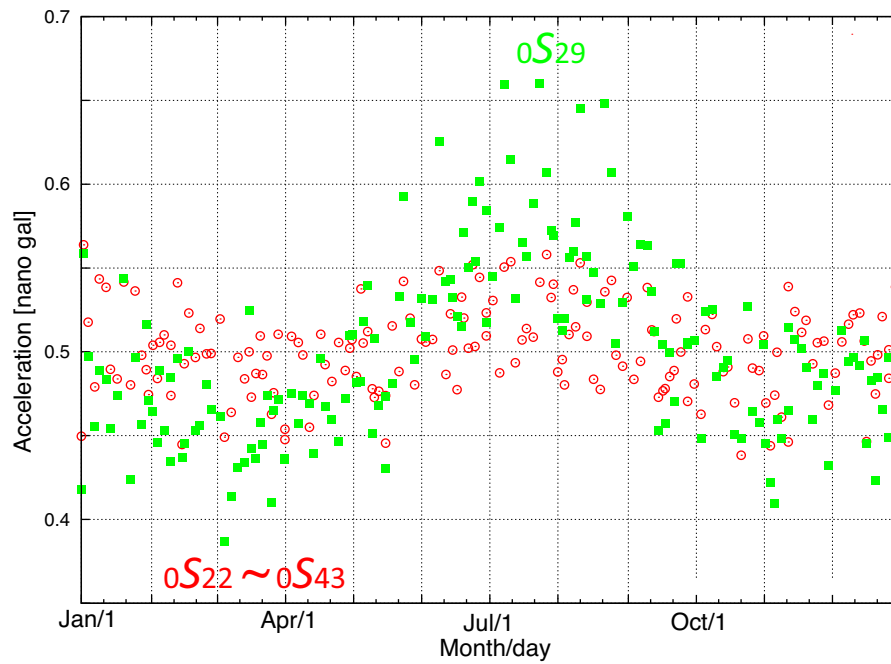


Figure 8: Temporal variations in modal amplitudes of fundamental spheroidal modes against days of the year. Data from 44 stations (Figure 1) from 1990 to 2011 was stacked. Red open circles show the mean modal amplitudes from  ${}_0S_{22}$  to  ${}_0S_{43}$  except for  ${}_0S_{29}$ . Green squares show the modal amplitudes of  ${}_0S_{29}$ , which is the acoustic coupling mode.

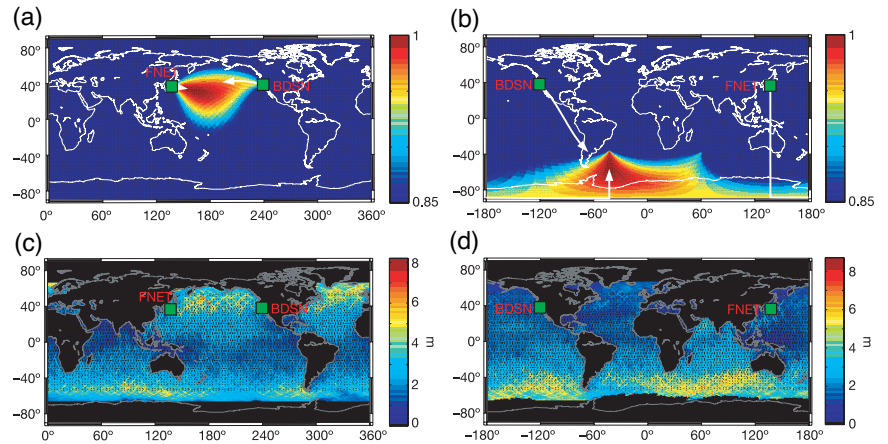


Figure 9: Comparison of seasonal variations in the distribution of hum-related noise (degree one only) and significant wave height in the year 2000. The directions corresponding to the mean amplitudes that are larger than 85% of the maximum are combined for the two arrays in (a) winter (b) and summer to obtain the region of predominant sources in each season. Arrows indicate the direction of the maxima. Both arrays are pointing to the North Pacific Ocean in the winter and to the southern oceans in the summer. Global distribution of significant wave height in the (c) winter and (d) summer averaged from TOPEX/Poseidon images for the months of January and July 2000, respectively. Black color in (c) and (d) indicates locations with no data. Taken from Rhie & Romanowicz (2004).

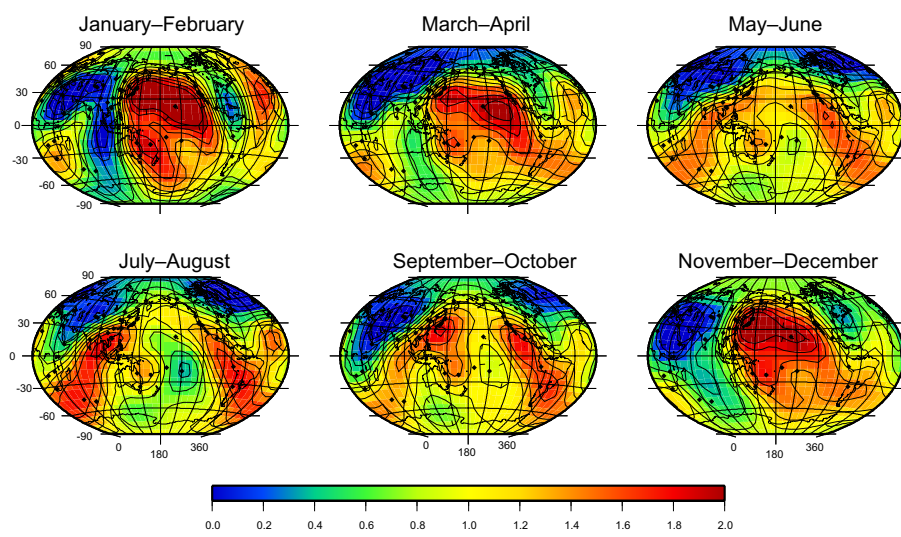


Figure 10: Spatial distribution of excitation sources estimated for every two months of the year. Indicated in color scale are amplitudes relative to the reference effective pressure model. Taken from Nishida & Fukao (2007).

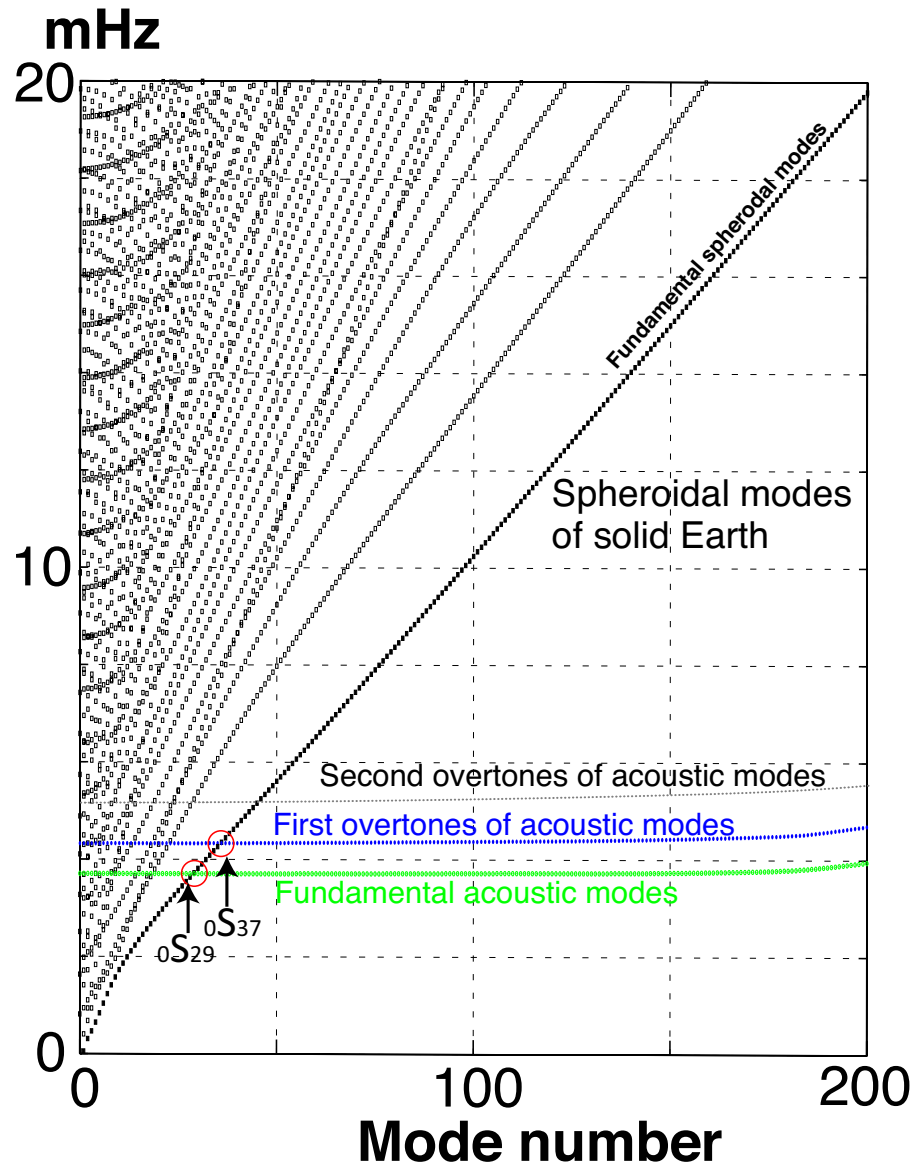


Figure 11: An overlay of dispersion diagrams of the solid earth and atmosphere.

The two circles show the two resonant frequencies.

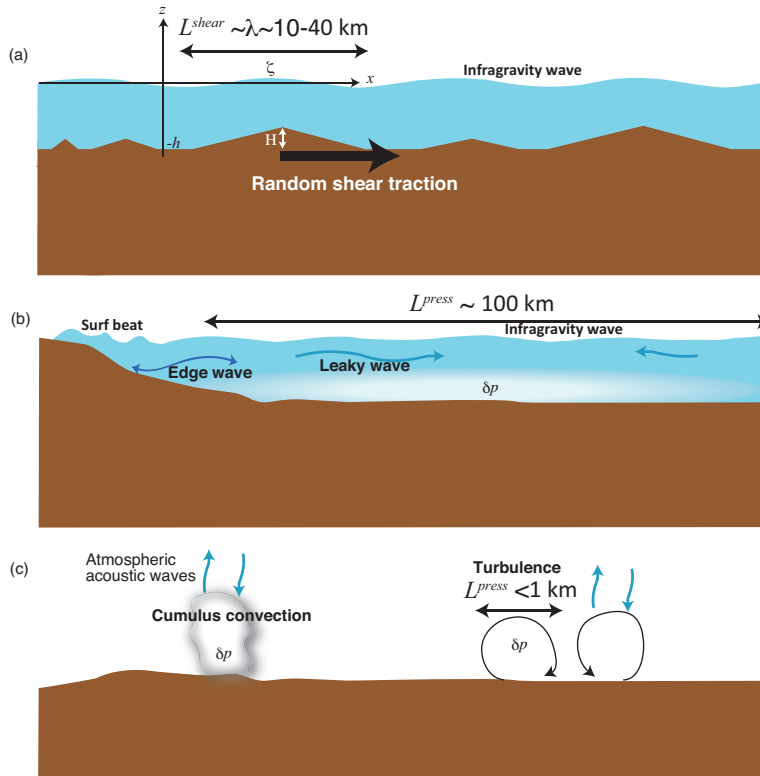


Figure 12: (a) A schematic of the topographic coupling between the ocean infragravity waves and the background Love and Rayleigh waves. The coupling occurs efficiently when wavelength  $\lambda$  of the infragravity waves at the frequency and the horizontal scale of the topography match each other.  $H$  is the height of the hill whose horizontal scale is  $\lambda$ ,  $\zeta$  is displacement amplitude of the sea surface. (b) A schematic of the nonlinear forcing of seismic modes by ocean infragravity waves in coastal areas. When two regular wave trains traveling in opposite directions with displacement amplitude of the sea surface interact, the second-order pressure pressure fluctuation  $\delta p$  with correlation length  $L^{press}$  excites background Rayleigh waves. (c) A schematic of the atmospheric excitation by cumulus convection or atmospheric turbulence in the troposphere. Random pressure fluctuation  $\delta p$  of cumulus convection or atmospheric turbulence with correlation length  $L^{press}$  excites background Rayleigh waves.